Efficient formability in radial-shear rolling of A2024 aluminum alloy with screw rollers.
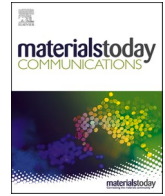
ELDEEB, I.S., HAWAM, A.A., NABHAN, A. and EGIZA, M.

2024

Efficient formability in Radial-Shear Rolling of A2024 aluminum alloy with screw rollers

Ibrahim Saad ELDeeb [a,*], Ahmed A. Hawam [a], Ahmed Nabhan [b], Mohamed Egiza [c,d,**]

[a] Department of Production Engineering and Mechanical Design, Faculty of Engineering, Tanta University, Tanta 31527, Egypt
[b] Production Engineering and Mechanical Design, Faculty of Engineering, Minia University, Minya 61111, Egypt
[c] Department of Mechanical Engineering, Kafrelsheikh University, Kafrelsheikh 33516, Egypt
[d] School of Engineering, Robert Gordon University, Garthdee Road, Aberdeen AB10 7GJ, UK

ABSTRACT

The Radial-Shear Rolling (RSR) process, commonly utilizing traditional conical rollers, encounters challenges in achieving optimal deformation in high-strength aluminum alloy A2024, vital for aerospace applications due to its exceptional strength-to-weight ratio. This study explores the potential of screw rollers to enhance RSR efficiency for A2024 aluminum, aiming to evaluate their impact on microstructure, mechanical properties, and key deformation parameters (force, temperature) compared to conical rollers. Employing a combined approach of finite element simulations and experiments with force analysis, the study assesses the effects of screw rollers in a two-pass RSR process. The findings reveal significant advantages with screw rollers, achieving a 15 % increase in equivalent strain compared to conical rollers, indicating enhanced material formability. Consistent temperature distribution across roller types ensures stable processing conditions. Screw rollers also demonstrate a 9 % reduction in force required during the second rolling pass, potentially reducing equipment load demands and enabling higher compression per pass for improved process efficiency. Additionally, a more uniform micro-hardness distribution suggests consistent mechanical properties with screw rollers compared to conical ones. These results highlight the potential of screw rollers to optimize RSR of A2024 aluminum, offering improved plastic deformation efficiency, temperature control, and potentially lower equipment loads. This advancement holds promise for a more efficient and cost-effective RSR process in producing high-quality A2024 aluminum components for aerospace and other demanding applications.

1. Introduction

Aluminum-copper-magnesium (Al-Cu-Mg) alloys, particularly A2024, play a vital role in aeronautics and aerospace due to their exceptional strength-to-density ratio and excellent corrosion resistance [1–3]. Hot extrusion followed by quenching and aging processes are the primary methods for shaping semi-finished products from these alloys, aiming to enhance hardness [4]. However, the increasing demand for improved strength-to-density ratio, bending stiffness, and corrosion resistance in A2024 poses challenges in specialized alloy manufacturing.

To address these challenges, the MISIS National Research and Technology University developed the Radial-Shear Rolling (RSR) method. This technique offers opportunities for seamless pipe and round bar rolling with varying diameters and grades [5,6]. RSR involves the

rotation and advancement of a preheated, circular billet by rolls with axes tilted relative to the pass line, inducing significant shear deformation [7].

However, a major challenge associated with RSR is the potential for internal fractures within the rolled material depending on the rolling parameters. This phenomenon, known as the "Mannesmann effect," can significantly compromise product strength and is difficult to detect [8]. Extensive research has been conducted since the 20th century to understand the mechanisms and develop methods to suppress these internal fractures [9,10].

Despite these challenges, RSR has proven to be a versatile technique applicable to various metallic materials. Round bars made of steel [11, 12], titanium alloys [13,14], magnesium alloys [15,16], aluminum alloys [17,18], and zirconium alloys [19] have all been successfully rolled

using RSR.

The core principle of RSR revolves around the specific rotating trajectory of the deformed metal, achieved by tilted angular cylinders. This trajectory creates significant tangential stresses, leading to both axial and circumferential flexing of the deformed band [20]. The resulting stress state during RSR resembles a combination of all-around compression and additional shear stress induced by the forced metal flow along a helical path within the rolled bar [21,22]. Studies have demonstrated the effectiveness of RSR in producing bars with enhanced mechanical properties while maintaining sufficient ductility, even for austenitic steel [23]. However, the impact of RSR on microstructure formation varies depending on the material. For instance, research on Al-Zn-Mg-Fe-Ni aluminum alloy bars revealed a gradient structure with an ultra-fine-grained surface layer and a coarse-grained core, along with an increase in microhardness at the center and decrease near the surface [24].

During metal forming processes, materials experience complex interactions of stress, strain, and temperature [25]. Understanding the behavior of metals and alloys, particularly during hot working, is crucial for achieving specific final product deformations. While traditional thermomechanical experiments like tensile, compression, and torsion tests offer valuable insights [26,27], they often deviate significantly from industrial practices. Industrial RSR involves significant zonal temperature changes and strain rates ranging from 0.1 to 100 s^{-1} due to varying work roll speeds [28]. This highlights the need to investigate the ideal deformation regime under parameters that replicate real-world industrial conditions. This study aims to explore these intricate dynamics, particularly focusing on A2024 aluminum, to contribute valuable knowledge for optimizing deformation processes in industrial applications.

High-strength aluminum alloys are critical materials in automotive, aerospace, and missile industries, constantly demanding improved properties to meet evolving technological needs [29,30]. RSR emerges as a preferred technique for producing long bars with a gradient functional structure in various materials due to its ease of implementation and adaptability. RSR machinery allows for the production of diverse product sizes by facilitating varying degrees of deformation in each pass. Prior research has extensively documented the underlying principles and key parameters of this method [31,32].

Investigations at NUST "MISIS" have demonstrated the effectiveness of RSR in enhancing the strength of alloys through microstructure refinement similar to severe plastic deformation (SPD) due to the high shear stresses applied to the workpiece surface layers [33,34]. This study delves deeper into these complexities, focusing on A2024 aluminum, to contribute insights into optimizing industrial metal forming processes.

Investigating the intricacies of RSR process parameters, including metal flow trajectories, equivalent strain distribution, slippage distribution, and force between rollers and workpiece, proves challenging through experimental means alone [35,36]. However, the Finite Element Method (FEM) emerges as a powerful solution facilitated by advanced computer simulation tools. FEM allows for comprehensive engineering studies on primary process parameters, circumventing limitations of time and cost. This is possible due to the availability of specialized software designed to simulate metal forming processes [37–39].

Several factors significantly influence the characteristics formed during RSR deformation, including the chemical composition of the material, strain rate, temperature, degree of deformation, roll profile, and the chosen deformation scheme of the initial workpiece. Additionally, the influence of these factors can vary considerably depending on the specific alloy. A thorough exploration of these complex interactions is essential for a nuanced understanding of the RSR process and its impact on material properties.

A recent development combining twisting deformation with RSR within a die has been proposed for energy-efficient production of hardened screw fittings. This innovative approach enables the formation of screw profiles in a single process [40]. Experimental production of screw fittings using this combined stand allowed researchers to investigate the effects of various process parameters on microstructure and mechanical properties.

Theoretical research plays a vital role in advancing any technological process by evaluating its performance under real-world conditions. In the context of RSR, FEM modeling stands out as the most comprehensive research approach. This method offers valuable insights into critical aspects such as the process feasibility under practical conditions, potential workpiece defects, and the equipment's capacity to handle anticipated loads. Furthermore, FEM allows for meticulous scrutiny of every process parameter at each stage within the workpiece, which can be challenging to achieve in practical scenarios.

This research aims to assess the effectiveness of screw rollers in improving the efficiency of the RSR process for high-strength aluminum alloy A2024, crucial for aerospace applications. Through a combined approach of FEM simulations and experiments, the study seeks to evaluate the impact of screw rollers on deformation parameters and material properties compared to conventional conical rollers. The goal is to optimize the RSR process for A2024 aluminum, enhancing material formability, process efficiency, and achieving consistent mechanical properties for high-quality component production.

2. Materials and methods

2.1. Experimental procedure

High-strength A2024 aluminum alloy was chosen for this study due to its widespread use in aerospace applications. Cylindrical billets with a diameter of 50 mm and a length of 300 mm were machined from commercially available A2024 aluminum bars. The chemical composition of the A2024 aluminum used is provided in Table 1.

The experimental setup for this study utilized custom-designed radial shear rolling mini-mills indicated in Fig. 1a. A constant feed angle (β) of 20° was maintained for all deformation processes across both roller types. However, the toe angle (δ) varied depending on the roller type and rolling pass. When conical rollers were used, the toe angle was set to 10° for the first pass and then reduced to 7° for the second pass. In contrast, screw rollers employed a consistent toe angle of 7° for both rolling passes. The work rollers were positioned symmetrically with a 120° step relative to the rolling axis. Each work roll had an exit angle on the calibration portion and an entry angle on the grip and reduction sections.

The computer model for this study consisted of three working rolls positioned symmetrically around the rolling axis, along with a workpiece whose axis ran parallel to the rolling axis (Fig. 1b). The figure also shows the point where the rolling axis and the roll axis intersect. Each roll was rotated around its own axis at a specific feed angle (β), and its rotational axis was tilted towards the rolling axis at a toe angle (δ). Due to the feed angle, the workpiece underwent a combined motion during deformation, rotating around its own axis while also flowing laterally along the rolling axis. Furthermore, it provides an overview of the entire RSR system and the configuration of the working rolls. To analyze the samples' hardness and microstructure throughout the deformation zone, sections were cut from the rolled bars, as depicted in Fig. 1c.

The distinctive design and geometry of the rollers played a critical role in achieving the desired deformation. This arrangement compelled the workpiece to follow a helical path while simultaneously decreasing its diameter. The rolling process employed a two-pass RSR method. In the initial pass, the diameter was reduced from 50 mm to 40 mm. Subsequently, in the second pass, the diameter was further reduced from 40 mm to 27 mm. A comparison between conical and screw rollers used in the RSR deformation process can be elucidated as follows: Two scenarios were proposed for investigation. In the first scenario, the rod underwent deformation using two passes of conical rolls. In the second scenario, the rod underwent deformation using two passes, one with

Table 1
Chemical composition of A2024 Aluminum (wt%).

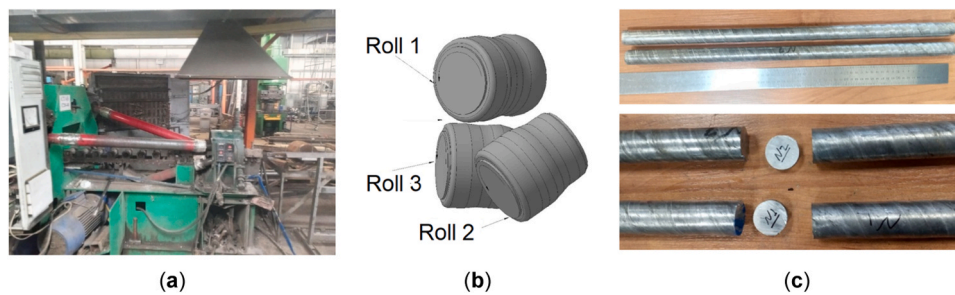| Cu	Mg	Mn	Zn	Ti	Fe	Si	Cr	Ni	Others	Al
3.8–4.9	1.2–1.8	0.3–0.9	≤0.25	≤0.15	≤0.50	≤0.50	≤0.1	≤0.01	≤0.15	90.7–94.7

Fig. 1. (a) Typical image of the Radial Shear Rolling (RSR) mini mill, (b) Schematic of screw rollers and Radial-Shear Rolling method, and (c) Rolled bars with corresponding cut sections.

special screw rolls and the other with conical rolls.

Prior to rolling, the billet was heated in an electric batch furnace to a uniform temperature of 400 °C (T_o) for 3 h. The rollers themselves remained unheated throughout the deformation process. Initial pushing was done manually. To maintain consistent temperature across the section, the bar was placed back in the furnace after each rolling pass.

RSR is a valuable method for producing metals with ultra-fine grains, finding practical applications in various industries. The process involves three conical rolls (Fig. 2) and three screw rollers (Fig. 3) rotating in the same direction [41]. These rolls intersect the rod's axis at a specific angle, causing it to both rotate and move in a translational direction during deformation. The feed angle (β) and toe angle (δ) of the three most common RSR roll mill configurations are illustrated. The feed angle is formed by the rolling axis and the projection of the roll axis onto a plane perpendicular to the line connecting the roll centers. This angle plays a crucial role by inducing axial movement in the metal. The toe angle, defined as the angle between the roll's axis and the plane perpendicular to its rotational axis, is another critical factor influencing the roll radius and peripheral velocity across the deformation zone's length. The development of shear strains within the rolled rod's cross-section depends on both the feed angle and the extent of rolling reduction applied to the rod's diameter.

Using SolidWorks software, 3D models of the original workpiece and working rolls were generated. Figs. 2a and 3a depict the basic structure of the RSR deformation zones. A specific calibration method based on the virtual modes' methodology was developed to simulate the RSR process. It's important to note the rolls with a substantial reduction section and a 20° feed angle β, as depicted in Figs. 2b and 3b. The rolls incorporate an entering area to facilitate gripping the workpiece and initiate rolling. The subsequent reduction zone features two taper angles, allowing for diameter reduction while maintaining a specific elongation ratio. A calibration zone on the exit side of the roll ensures the bar's final round cross-section. Tracking locations for analyzing parameters within the deformation zone are identified. These four tracking points are positioned at the middle of the workpiece length, at distances of 0(C), 0.4 R, 0.8 R, and R from the workpiece axis.

The initial cylindrical workpiece dimensions were 300 mm in length and 50 mm in diameter. Three rolling tools were equidistantly positioned around the rolling axis at 120° intervals. The feed angle, β, was maintained at 20°, while the toe angle, δ, was varied between 10° and 7° (Figs. 2c and 3c). These parameter selections were based on previous research [42,43] indicating optimal feed angle and toe angle ranges of 18°-24° and ≤10°, respectively. The axial position of the rolls was adjusted to achieve the target bar diameter in accordance with the desired elongation ratio.

The rolling process involved two distinct stages, regardless of whether conical or screw rollers were used. In the first pass, the diameter was reduced from 50 mm to 40 mm, achieving an elongation ratio of μ = 1.5. This ratio was repeated in the second pass, further reducing the diameter from 40 mm to 27 mm while maintaining μ = 2.3. Utilizing these specific elongation ratios in each pass helped control deformation heating, ultimately resulting in a bar with the desired geometrical parameters.

2.2. Finite element model

The RSR process is complex, and directly measuring parameters like temperature, velocity, stress, and strain under laboratory or production
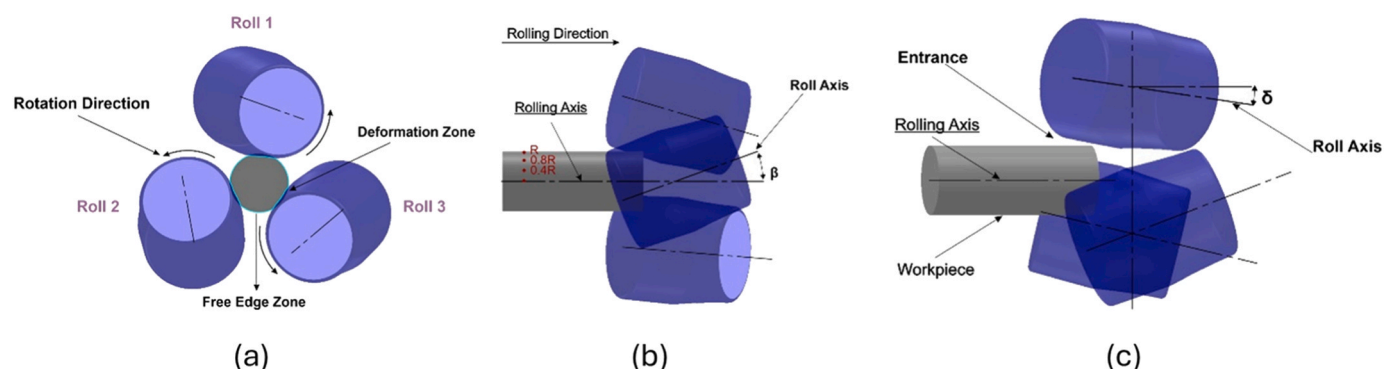

Fig. 2. RSR setup with conical rollers: (a) Schematic with three conical rollers, and (b,c) 3D models of workpiece and calibrated conical rolls.
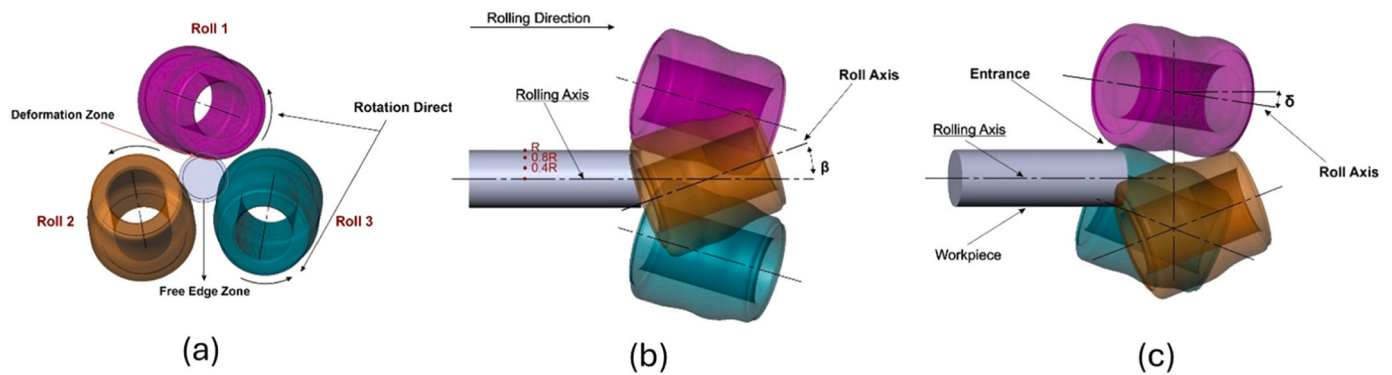
Fig. 3. RSR with screw rollers: (a) Principal scheme, (b,c) 3D models of workpiece and screw rolls.

conditions is challenging. Previous studies have utilized computer modeling to investigate RSR with screw rollers on aluminum alloys such as AA7075 and A1050 [18,25,44]. This study adopted a similar computational approach to analyze stress, strain, and temperature distributions in A2024 aluminum, while microhardness and microstructure were determined experimentally. A 3D model of the rolling setup was constructed using SolidWorks and then simulated using the QFORM finite element software. This software accurately represented the rolling process, with the rolls rotating at a constant speed of 40 rpm around a shared axis and positioned according to specific toe and feed angles.

The QFORM software includes a comprehensive database of chemical, mechanical, and physical properties for common industrial materials. Material data for the widely used A2024 aluminum alloy was extracted from this database. Fig. 4 presents the stress-strain curves for A2024 at various temperatures (300, 350, 400, 450 °C) and strain rates (0.1, 1, and 10 s^{-1}). The thermal properties of A2024, including specific heat, thermal conductivity, and thermal expansion, were incorporated into the FE model (see supplementary materials). The simulation considered heat transfer between the workpiece, its surroundings, and the rolling tools. Two consecutive rolling passes were simulated at a constant temperature of 400 °C, with the billet initially at a uniform temperature of 400 °C. A heat transfer coefficient of 10,000 W/m^{2}K was applied between the tools and the billet.

The simulation results facilitated the examination of temperature distribution within the deformation zone following the RSR process and allowed for the analysis of the equivalent strain (ε) across the bar's cross-section. In QFORM, equivalent strain is calculated by numerically integrating the strain rate intensity for each mesh node of the workpiece along the trajectory of the deformed metal particles. Four specific locations within the bar were chosen for analysis (P1: center, P2: 0.4 radius, P3: 0.8 radius, P4: surface). The simulation employed a refined

mesh size of 2 mm. To ensure mesh convergence, the mesh size was gradually reduced until the stress distribution and levels stabilized, indicating an appropriate mesh size. Eq. (1) illustrates the formula used in QFORM for calculating the equivalent strain (ε):

$$\varepsilon = \sum_t \varepsilon \Delta t_n \tag{1}$$

Where n represents the number of time steps in the calculation and Δt_n defines the step calculation time.

The simulation ultimately created a model for the RSR forming process involving three RSR screw mills. As depicted in Fig. 5, this process rolls a billet through the mills, generating a screw profile on the external surface of the cylindrical billet. The application of deformation forces occurs as the billet exits the deformation zone, acting along its longitudinal axis at a predetermined angle set by the configuration of the screw mill. Table 2 summarizes the key parameters used for the modeling process.

2.3. Microstructure and hardness analysis

Microhardness measurements were conducted using Vickers technique via "Metkon MH-6" universal microhardness tester. The tests employed a load of 1 kg applied for a dwell time of 5 seconds. These measurements were performed at the midsection of the rolled bars. Microhardness was measured across the entire cross-section, with three measurements taken at each point for increased accuracy.

To understand the microstructural changes induced by the RSR process, the cross-sections of the bars were analyzed. Specimens were prepared for analysis by grinding, polishing, and etching with Keller's reagent (190 ml water, 3 ml hydrochloric acid, 2 ml 48 % hydrofluoric acid). The microstructure of these prepared specimens was then
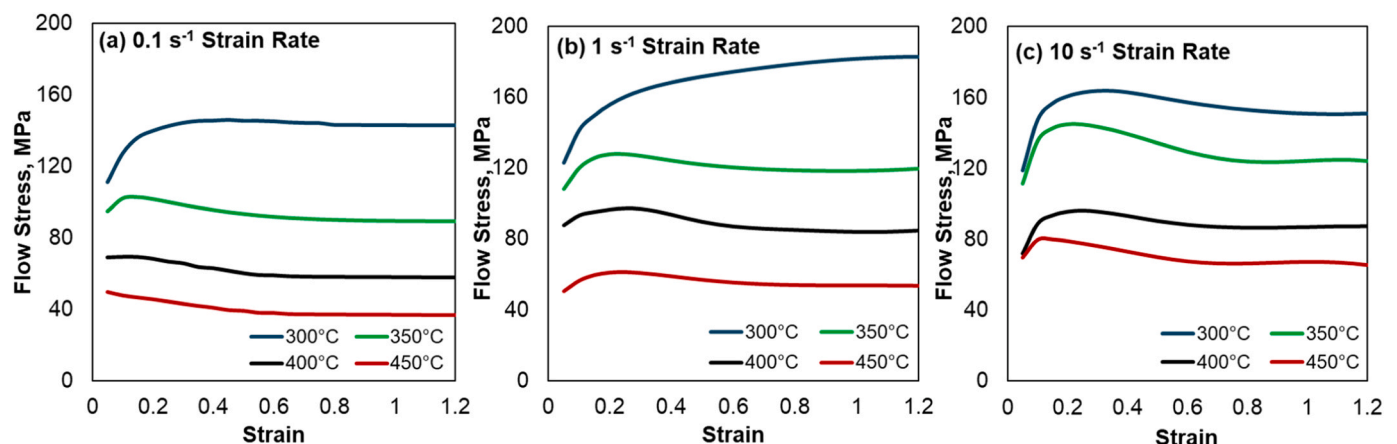

Fig. 4. Stress–strain curves of the A2024 aluminum alloy at different temperatures (300, 350, 400, 450) and strain rates: (a) 0.1, (b) 1, and (c) 10 s^{-1}.
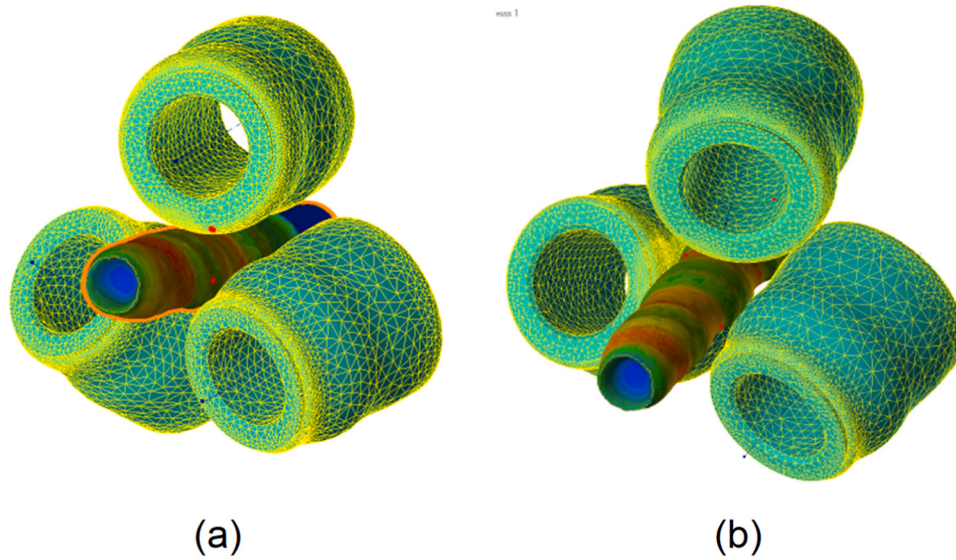
Fig. 5. Various perspectives depicting the modeling of screw mills in the RSR deformation process, illustrating the three RSR rolling profiles.

Table 2
Modeling parameters for the RSR process.

Parameter	Measurement units	Value
Toe angle δ	(°)	10, 7
Feed angle β	(°)	20
Material of the roll	-	40Cr
Temperature of the roll	(°C)	25
Ambient temperature	(°C)	25
Friction factor (Siebel Law)	-	1.0
The heat transfer coefficient (α) between the material and the tool	(W/K·m2)	10,000
The heat transfer coefficient (α air) between the material and the air	(W/K·m2)	30
Workpiece mesh adaptation factor	-	2

examined using a Carl Zeiss Axio Lab.A1 optical microscope.

3. Results and discussion

3.1. Equivalent strain distribution

Fig. 6 illustrate how equivalent strain (ε), a crucial indicator of plastic deformation in metal forming processes [45,46], is distributed across the length (longitudinal) and cross-section of the bar after RSR process. The chosen rolling shape significantly impacts the distribution of equivalent strain, which in turn affects the localized contact stress during the heating process.

The simulation data reveals that the maximum values of equivalent strain exhibit an increasing trend along the gradient for all analyzed rolling shapes. However, conical rolls stand out by creating a more pronounced and uniform gradient of equivalent strain from the surface towards the center along the bar's length (longitudinal section). In contrast, for screw rolls, the equivalent strain near the surface displays variations that depend on the degree of compression applied.

The different roller profiles and rolling process parameters apparently affect the equivalent strain distribution within the bar during RSR process. The equivalent strain, a measure of plastic deformation, varies across the bar's cross-section, leading to diverse microstructures [46]. Four specific locations within the bar were chosen for analysis (P1: center, P2: 0.4 radius, P3: 0.8 radius, P4: surface) as shown in Figs. 2b and 3b. Additionally, Fig. 7 and Fig. 8 track the changes in equivalent strain at these points (P1-P4) during the rolling process.

The highest temperatures occur in areas with the most concentrated strain and stress [28], particularly near the surface (point P4). This is because each roll pass in the open deformation zone creates significant localized heating. As point P4 travels through the non-contact zone between the rolls, its temperature fluctuates greatly due to the combined effect of high strain and reduced contact.

The type of roller profile significantly impacts the equivalent strain distribution. Screw rollers, compared to conical rollers, lead to a higher equivalent strain at the surface during the reduction zone (evident in the
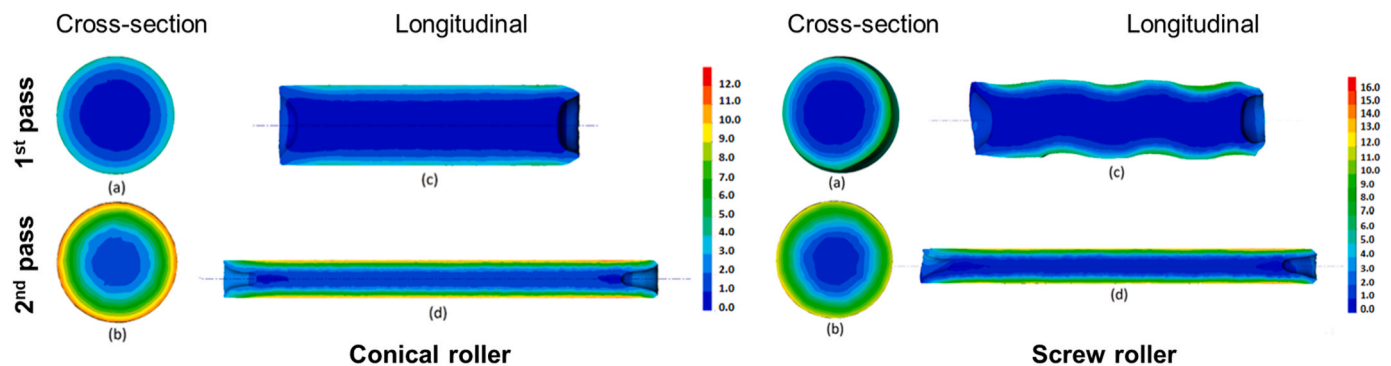

Fig. 6. Equivalent strain distributions across the cross-sections (a,b) and longitudinal (c,d) of the bar after RSR with conical and screw rollers during the (a,c) first pass, and (b,d) second pass.
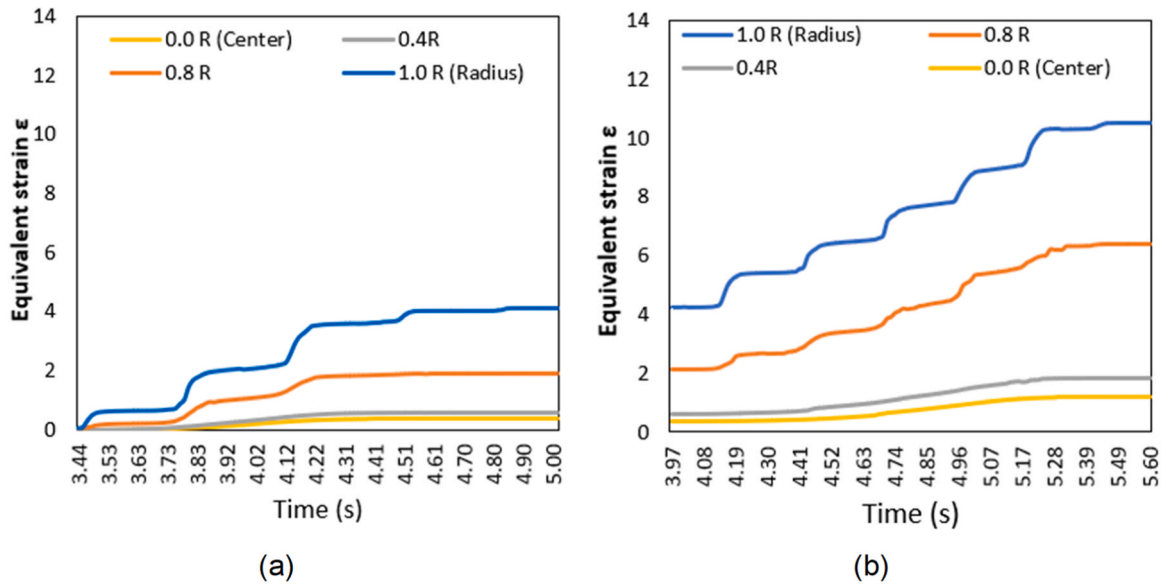
Fig. 7. Equivalent strain distribution along the deformation zone's length at various positions from centers with conical rollers: (a) First pass, (b) Second pass.
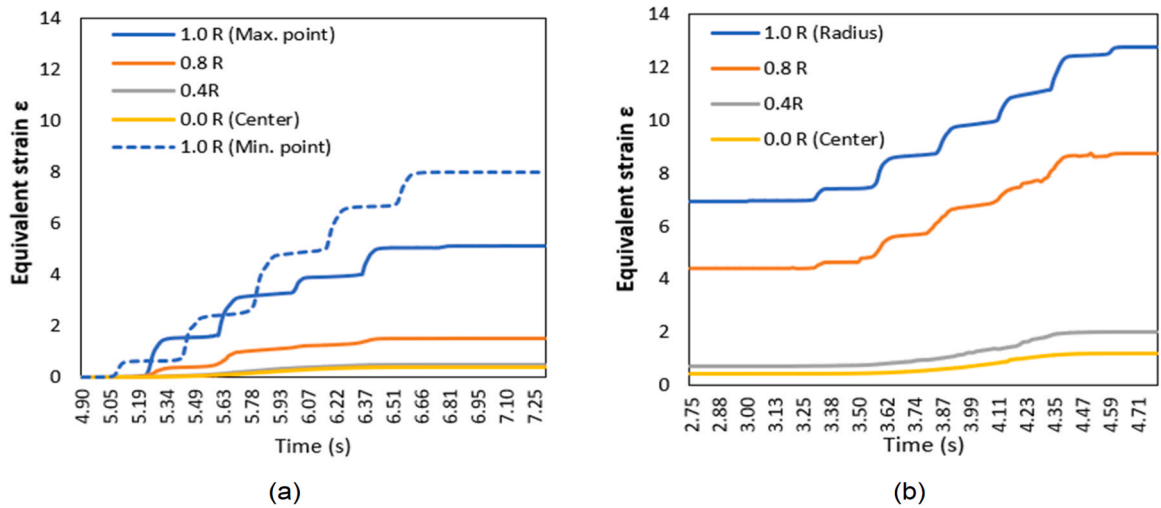

Fig. 8. Equivalent strain distribution along the length of the deformation zone at various positions from the center using screw rollers: (a) first pass, (b) second pass.

step-like increases in Fig. 8). In fact, screw rollers achieve a 27 % and 24 % higher equivalent strain than conical rollers in the first and final passes, respectively. This highlights the effectiveness of screw rollers in enhancing overall equivalent strain during RSR process.

While the interplay between roller profiles, particularly screw and conical rollers, can be complex and difficult to predict analytically, simulations offer valuable insights during the manufacturing process. By analyzing equivalent strain, a key factor influencing material properties, simulations can help predict final product characteristics. This is especially important in multi-pass rolling processes, where monitoring equivalent strain after each pass is crucial. As shown in Figs. 7 and 8, equivalent strain (ε) and its change ($\Delta\varepsilon$) are tracked across various locations within the bar (P1-P4). $\Delta\varepsilon$ is calculated by the difference between the center (P1) and surface (P4) during deformation.

The RSR process creates a gradient of equivalent strain across the rolled product. The outer zone, experiencing concentrated shear strains, exhibits the highest values (ε). Conversely, the inner zone, affected by the reduction in cross-sectional area, has the lowest equivalent strain. The type of roller profile significantly impacts this gradient. Screw rollers, compared to conical rollers, lead to a steeper gradient with a 15 %

higher maximum equivalent strain on the outer surface during the first pass. This highlights the significant role of roller profiles in influencing the final strain distribution. The high level of friction between the rolls and the billet concentrates strain near the surface, leading to a significant difference in equivalent strain between the outer and central regions of the bar.

3.2. Temperature analysis

Despite using different roller profiles (conical and screw), which resulted in varying levels of strain, the temperature distribution within the rolled bar during the RSR process displayed consistent patterns, as illustrated in Figs. 9–11. Temperature, a critical parameter in metal forming, was observed across both the length and cross-section of the bar. These findings suggest that the roller profile has a limited impact on overall temperature changes. Surface temperature, primarily influenced by contact with the cold rolls, exhibited the most significant fluctuations. In contrast, the bar's interior experienced a steady temperature rise due to deformation heat. Notably, the temperature distribution remained consistent throughout multiple rolling passes, irrespective of
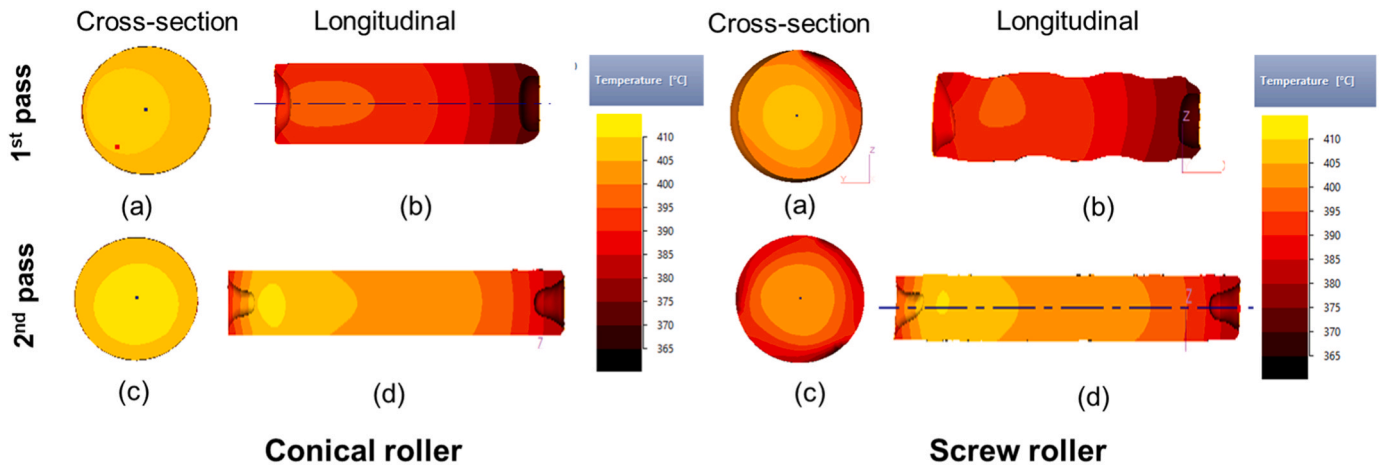
Fig. 9. Temperature distributions across the cross-sections (a,b) and longitudinal (c,d) of the bar after RSR with conical and screw rollers during the (a,c) first pass, and (b,d) second pass.
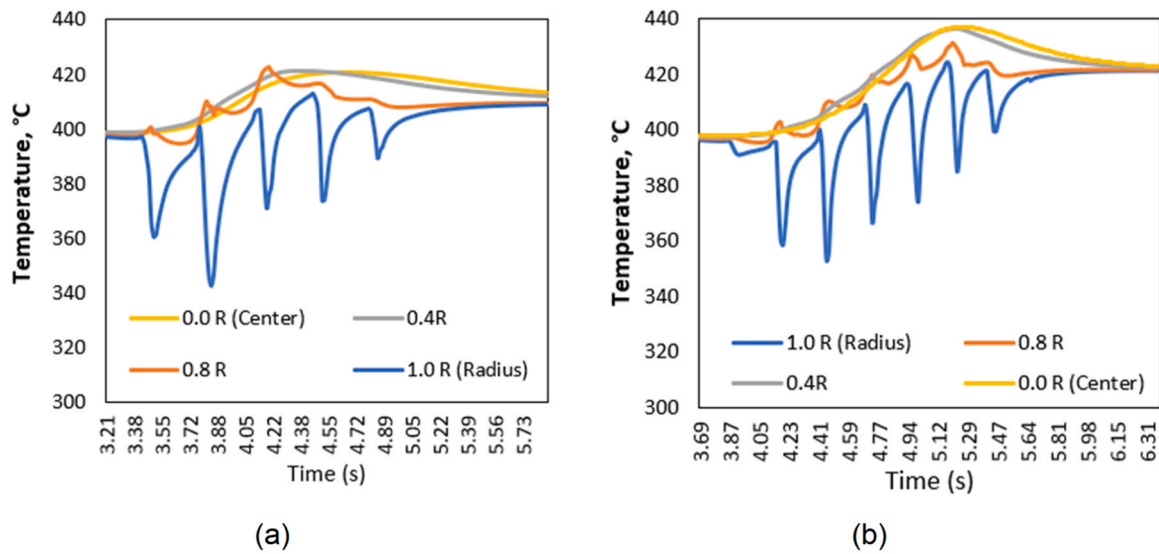

Fig. 10. Temperature distribution along the length of the deformation zone at various positions from the center using conical rollers: (a) first pass, (b) second pass.

the roller type.

During the RSR process, the interaction between the tracked surface element of the bar and the relatively cooler rolls generates temporary dips, or local minimums, in the temperature curves. The frequency of these dips corresponds to the total number of deformation cycles undergone by the bar. Interestingly, the data suggests that as the temperature decreases further with each cycle, indicated by deeper dips, there is an increase in the number of cycles. This observation may be attributed to a decrease in the angle of the surface trajectory during rolling. A shallower angle could potentially result in more frequent contact between the surface and the rolls, leading to more frequent cooling events and a higher number of dips observed in the temperature profile.

3.3. Force analysis

The force exerted on the rolls during RSR follows a distinct pattern, as shown in Fig. 12a. As the billet enters the rolls, the force gradually increases until the metal exits and a rear shrinkage cavity forms. This is followed by a progressive decrease in force until it reaches zero. Interestingly, a noticeable and sharp jump in force is observed just as the billet exits the rolls.

The analysis also revealed differences in force based on the roller

profile used. In the initial pass, screw rolls exhibited an average of 11 % higher force compared to conical rolls. This is likely due to variations in the contact surface shape caused by the different roll profiles. However, during the second pass using bars processed with screw rolls, the average roll force decreased by 9 %. This reduction can be attributed to the smaller diameter rolls used in the second pass. This approach not only minimizes the load on the equipment but also allows for higher compression per pass in the second stage, improving the overall efficiency of the RSR process.

Fig. 12b details the force distribution throughout the RSR process. As the rolls first capture the billet, the force gradually increases. This rise continues until the metal exits the rolls and a rear shrinkage cavity form, at which point the force progressively decreases to zero.

The figure reveals key findings regarding roller profile selection. When using conical rollers for both passes, the average force during the first pass is 25 % higher than the second. In contrast, employing a screw roller in the first pass followed by conical rollers in the second leads to a more significant 39 % difference in force between the passes. This highlights the impact of roller profiles: screw rollers in the first pass contribute to a higher initial force.

However, the use of smaller diameter rolls in the second pass, regardless of the first pass roller profile, proves advantageous. This
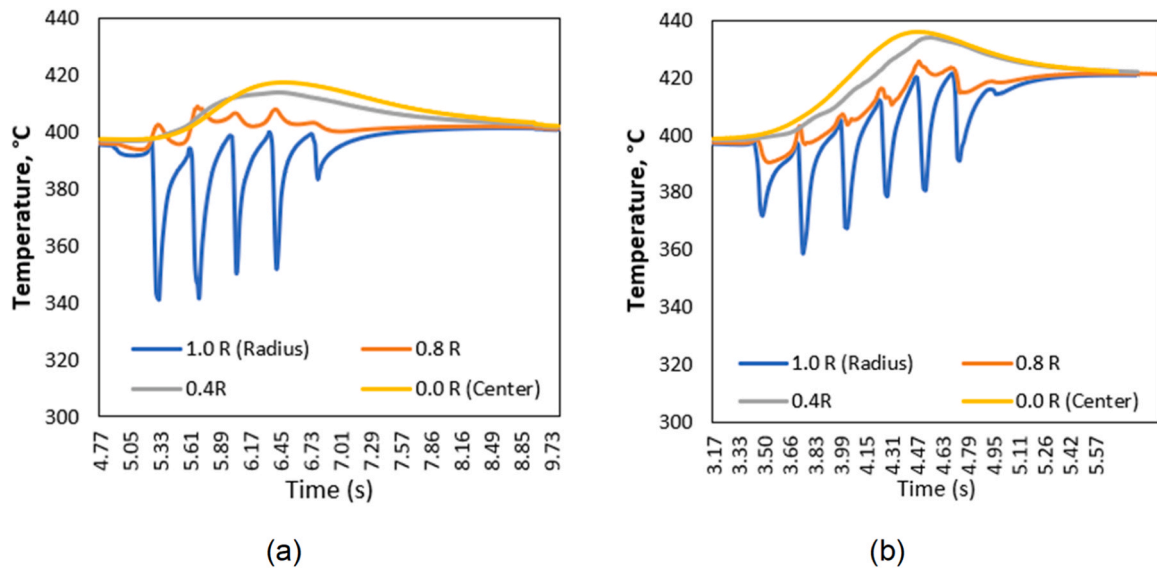
Fig. 11. Temperature distribution along the length of the deformation zone at various positions from the center using screw rollers in the (a) first pass, and (b) second pass.
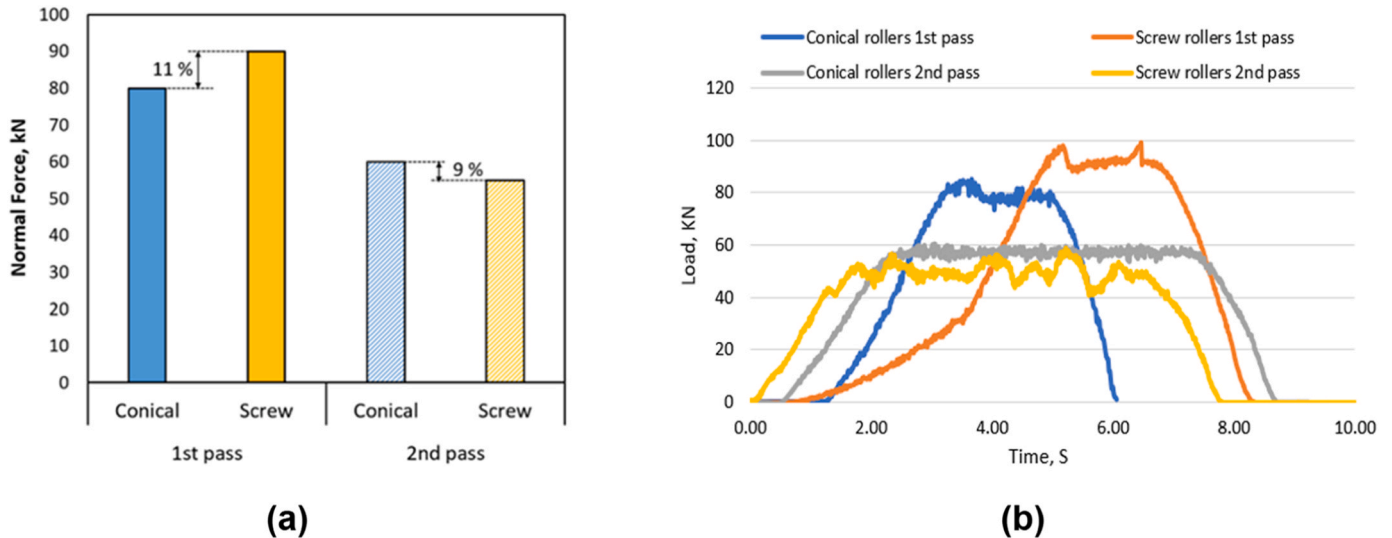

Fig. 12. a) Force during the deformation process of A2024 utilizing conical and screw rollers in RSR, b) Radial force graphs during the first and second deformation passes of A2024 using conical and screw rollers in the radial-shear rolling process over time.

approach effectively reduces the average force on the equipment, minimizing equipment load. Additionally, it allows for achieving higher compression per pass in the second stage, improving the overall efficiency of the RSR process.

The concept of radial force, acting perpendicular to the roll axis, is also depicted in the graph. It progresses through three distinct phases: the initial increase as the rolls capture the metal, a plateau representing a stationary stage, and a final decrease to zero force as the metal exits the deformation zone.

3.4. End-tightening patterns and associated defects

The non-uniform metal flow during RSR leads to distinct end-tightening patterns on the bars, highlighting the uneven deformation throughout the process [47]. These patterns often manifest as helical grooves on the surface, caused by twisting and the spiral movement of the material. These observations suggest potential improvements, such as extending the sizing section or adjusting the transition areas between forming and fitting sections in the rollers.

An additional concern is the development of an "end concave" defect at both the head and tail of the rolled pieces. The depth of this concavity is affected by the roller profile used. With two passes using conical rollers, the average depth is 29.01 mm. This depth is slightly reduced to 27.64 mm when a screw roller is used in the first pass followed by a conical roller in the second pass. This difference arises because the metal near the surface flows faster than the metal at the center during deformation.

Visually, these end-tightening patterns are evident. Bars rolled with two conical roller passes exhibit a more elongated shape in the longitudinal-transverse plane, with an average depth of 29.01 mm (see Fig. 13) [47]. Conversely, bars processed with a screw roller in the first pass and a conical roller in the second pass show less elongation and a shallower concave defect, averaging around 27.64 mm.

The presence of these concave defects can impact material utilization during production. This highlights the importance of addressing them through further processing steps. It's important to note that no central

Fig. 13. End-tightening depth variation in A2024 bars during RSR with different roller profiles: (a) Sample sectioning with groove dimension, (b) General view of the sectioning process.

defects were observed in either the longitudinal or transverse sections of the rolled bars. Overall, these findings contribute to a comprehensive understanding of how end-tightening depth and associated defects evolve during RSR deformation.

3.5. Deformation parameters analysis in RSR

This study investigated the influence of various process parameters on the material characteristics during RSR, with a particular focus on how equivalent strain (ε) affects these properties. Notably, RSR, which involves severe plastic deformation, creates a non-uniform distribution of equivalent strain across the rolled product [48,49].

The highest equivalent strain is observed in the outer zone of the workpiece, where concentrated shear strains occur. Conversely, the inner zone experiences lower ε values, primarily due to the reduction in the bar's cross-sectional area during deformation.

The type of roller profile used plays a significant role, especially in the first pass. Specific roller profiles can significantly increase the maximum equivalent strain values on the outer deformed surface, with minimal impact on the minimum values at the bar's center.

These observations highlight the complex interplay of factors. The rheological component, particularly the plastic deformation energy associated with flow stress and strain rate, influences the heating process during deformation. The study suggests a self-reinforcing system: the non-uniform distribution of equivalent strain (ε) leads to non-uniform deformation heating. This, in turn, reduces the metal's resistance near

the surface layers, allowing for even higher strain accumulation in these areas and a subsequent rise in maximum strain values. This amplification effect creates a heightened deformation-temperature gradient, showcasing the intricate dynamics at play in the RSR process [48,49].

4. Microstructure and hardness distribution

Fig. 14 explores the impact of different roller configurations on microhardness distribution across the cross-section of 27 mm bars processed using RSR. Bars rolled with conical rollers in two passes exhibit a higher overall microhardness compared to those subjected to a single pass with screw rollers. The observed pattern shows a clear trend: microhardness is highest near the bar's surface and gradually decreases towards the center.

For example, with conical rollers, surface microhardness reaches around 75–80 HV, while the center is slightly lower at 70 HV. Conversely, screw rollers result in a surface hardness of approximately 70 HV, with the center even lower at about 65 HV.

A significant advantage of screw rollers is the reduced variation in hardness across the bar's cross-section. As shown in Fig. 14b, conical rollers lead to a 4 % difference between maximum and minimum hardness values, whereas screw rollers achieve a minimal 1 % difference. This indicates a more uniform hardness distribution (1 % variation) when using screw rollers in RSR.

Moving beyond hardness, microstructure analysis is crucial. Fig. 15 presents a detailed examination of microstructure after two RSR passes
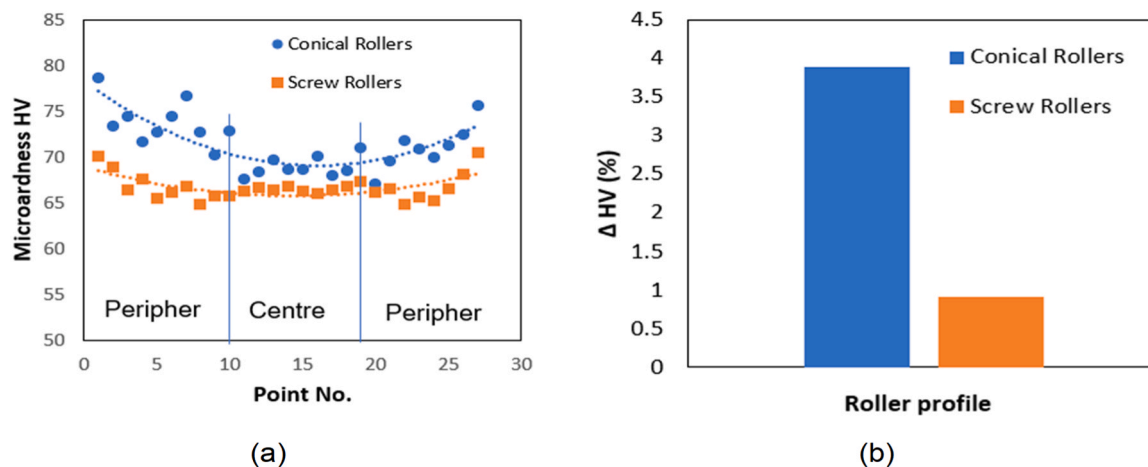

Fig. 14. (a) Microhardness distribution and mechanical properties across the cross-section, and (b) Microhardness variation in A2024 induced by conical and screw rollers.
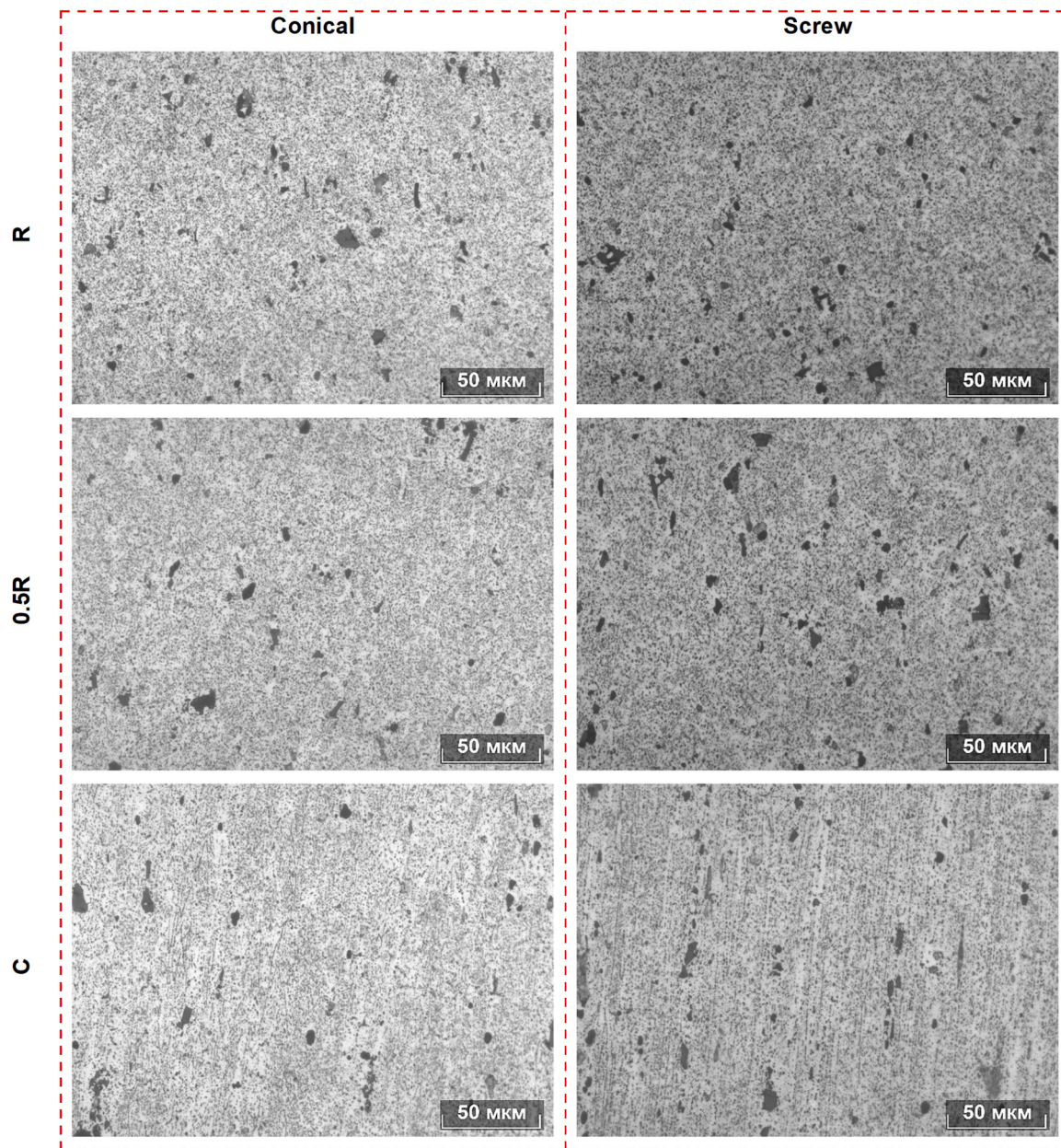
Fig. 15. Microstructure of A2024 bars processed via RSR using conical and screw rolls.

using different roller profiles. The analysis focused on three distinct zones: near the surface, halfway through the radius (0.5 R), and the bar's center. The findings reveal a consistent microstructure characterized by a uniform distribution of fine particles within the aluminum matrix and the presence of larger, darker secondary phase particles. Notably, no significant differences in microstructure were observed between bars processed with conical or screw rollers.

One interesting observation is particle morphology. Particles near the surface and up to the middle of the radius appear more rounded. In contrast, the axial part of the bars exhibits signs of deformation texture, with particles aligning along the rolling direction. These microstructure images suggest that either the elongation ratio in the first pass might be insufficient to reveal microstructural differences between roller profiles, or the second pass might even out these variations.

The potential of RSR using a novel screw roll profile is explored to achieve a desirable grain structure in a high-strength aluminum alloy. While traditional RSR processes can achieve an ultra-fine grain structure [40,50], the grain size distribution is often uneven across the

workpiece's cross-section, with the finest grains concentrated near the surface.

The findings demonstrate that combining RSR with this new screw roll profile after a single deformation cycle effectively creates the conditions for an ultra-fine grain structure throughout a larger portion of the material. Additionally, this approach results in a significantly reduced gradient in grain size across the cross-section compared to traditional methods.

This research suggests that RSR using a screw roll profile can be a viable technique for producing a gradient grain structure in this specific high-strength aluminum alloy. This gradient structure offers a combination of beneficial mechanical properties. An equiaxed fine-grained structure was formed near the surface, likely due to the high levels of stress and strain during dynamic recrystallization in this region. This explains the observed decrease in microhardness in this area, which is characteristic of a recrystallized structure.

Conversely, the area around the center of the sample experiences lower stresses and strains, leading to a non-recrystallized fibrous grain

structure with a corresponding increase in hardness. The microhardness distribution and structural analysis support the conclusion that employing a special screw roll design in RSR is an effective method for achieving a desirable gradient grain structure in this high-strength aluminum alloy.

5. Conclusion

This study addressed limitations in the Radial-Shear Rolling (RSR) process for high-strength aluminum alloy A2024, critical for aerospace applications due to its exceptional strength-to-weight ratio. Conventional conical rollers frequently encounter difficulties in achieving optimal deformation, thereby impeding process efficiency and the attainment of desired material properties. To address this issue, a combined approach involving simulations and experiments, including force analysis, temperature distribution analysis, microhardness evaluation, and end-tightening variation analysis, was employed. The primary objective was to optimize the deformation process and enhance process efficiency by introducing screw rollers.

The results underscore a clear relationship between roller profiles and microhardness distribution. In a two-pass RSR process with conical rollers, there was a higher average microhardness (around 75–80 HV near the surface) compared to a single pass with screw rollers (approximately 70 HV near the surface). This discrepancy in average microhardness (4 % variation for conical vs. 1 % for screw rollers) emphasizes the potential for tailored mechanical properties through specific roller profile selection. Moreover, the dynamics of force distribution further support the advantages of screw rollers. Although an initial 11 % higher force on the roll was observed during the first pass with screw rollers, a subsequent 9 % reduction occurred in the second pass. This reduction suggests the potential for reduced equipment load and achieving higher compression per pass, offering practical benefits for industrial settings. Visual observations of end-tightening variations provided additional insights into the nuanced effects of roller profile on deformation behavior. Screw rollers yielded a distinct end-concave defect with an average depth of around 27.64 mm, while conical rollers produced a more elongated form with an average depth of approximately 29.01 mm.

These observations contribute to a comprehensive understanding of the interplay between microstructural, mechanical, and thermal aspects of RSR. Furthermore, the study revealed that screw rollers induce higher equivalent strains on the surface, confirming their role in influencing the deformation process. Notably, changes in roll profile had minimal impact on the temperature field during RSR, suggesting the process's robustness under different roller configurations. This research lays a foundation for optimizing the RSR technique for A2024 aluminum, highlighting the practical feasibility and potential industrial applications of screw rollers in achieving desired material properties with enhanced efficiency. Further studies incorporating diverse microstructural analysis techniques and scaling up to industrial-scale applications are recommended to refine and validate these findings.

CRediT authorship contribution statement

Mohamed Egiza: Writing – review & editing, Supervision, Project administration. **Ibrahim Saad ELDeeb:** Writing – original draft, Methodology, Formal analysis, Data curation, Conceptualization. **Ahmed A. Hawam:** Visualization, Validation, Methodology. **Ahmed Nabhan:** Visualization, Validation, Methodology, Formal analysis.

Declaration of Competing Interest

The authors declare that they have no known competing financial interests or personal relationships that could have appeared to influence the work reported in this paper.

Data availability

Data will be made available on request.

Appendix A. Supporting information

Supplementary data associated with this article can be found in the online version at doi:10.1016/j.mtcomm.2024.110241.

References

[1] L. Troeger, E.J.M.S. Starke Jr, E. A, Microstructural and mechanical characterization of a superplastic 6xxx aluminum alloy, 277(1-2), 2000, 102-113. https://doi.org/10.1016/S0921-5093(99)00543-2. .

[2] A. Heinz, A. Haszler, C. Keidel, S. Moldenhauer, R. Benedictus, W.S. Miller, Recent development in aluminium alloys for aerospace applications, Mater. Sci. Eng. A 280 (1) (2000) 102–107, https://doi.org/10.1016/S0921-5093(99)00674-7.

[3] T. Warner, Recently-developed aluminium solutions for aerospace applications, Mater. Sci. Forum Trans. Tech. Publ. (2006) 1271–1278, https://doi.org/10.4028/www.scientific.net/MSF.519-521.1271.

[4] G.E. Totten, D.S. MacKenzie, Handbook of aluminum: vol. 1: physical metallurgy and processes, CRC press2003. https://doi.org/https://doi.org/10.1201/9780203912591.

[5] B. Romantsev, A. Goncharuk, A. Aleshchenko, Y. Gamin, M.J.T.I.Jo.A.M.T. MintakhanovDevelopment of multipass skew rolling technology for stainless steel and alloy pipes' production, 972018, , 3223–3230, 10.1007/s00170-018-2134-3..

[6] E. Ibrahim, I. El-Deeb, M.R. Mohamed SalemThe Effect of Strain Rate on Electrical and Mechanical Characteristics of Pure Aluminum Using Equal Channel Angular Pressing (ECAP), 7(5) (2023) 37-44. https://doi.org/10.21608/erjeng.2023.241762.1276. .

[7] K. Nakasuji, K. Kuroda, C.J.Ii HayashiDevelopment and features of rotary reduction mill, 31(6) (1991) 620-627. https://doi.org/10.2355/isijinternational.31.620.

[8] E.J.Jo.A.M. ErmanThe effect of processing parameters on the propensity for central fracturing in piercing, 4(4), 1987, pp. 331-341. https://doi.org/10.1016/0378-3804(87)90032-5.

[9] M. Novella, A. Ghiotti, S. Bruschi, P.J.Jo.M.P.T. BarianiDuctile damage modeling at elevated temperature applied to the cross wedge rolling of AA6082-T6 bars, 222, 2015, pp. 259-267. https://doi.org/10.1016/j.jmatprotec.2015.01.030.

[10] Z. Pater, J. Tomczak, T.J.I.Jo.M.S. BulzakEstablishment of a new hybrid fracture criterion for cross wedge rolling, 167 (2020) 105274. https://doi.org/10.1016/j.ijmecsci.2019.105274.

[11] A. Naizabekov, S.N. Lezhnev, E. Panin, I. Volokitina, A.J.M. KasperovichRealization of the innovative potential of radial-shear rolling for forming the structure and mechanical properties of AISI-321 austenitic stainless steel, 2021. https://doi.org/10.1590/S1517-707620210003.13018.

[12] N. Surikova, V.E. Panin, N. Narkevich, A.I. Gordienko, N.Y. SurikovHardening austenitic Stainl. Steel Intensive Cross screw Roll, 2018. 10.1063/1.5083539..

[13] B.V. Karpov, P.V. Patrin, S.P. Galkin, E.A. Kharitonov, I.B.J.M. KarpovRadial-Shear Rolling of Titanium Alloy VT-8 Bars with Controlled Structure for Small Diameter Ingots (≤200 mm), 61, 2018, pp. 884–890, 10.1007/s11015-018-0581-6..

[14] X. Ding, L. Sun, X. Huang, Z. Zhao, Research on three-roll screw rolling process for Ti6Al4V titanium alloy bar, High Temp. Mater. Process. 38 (2019) (2019) 178–182, https://doi.org/10.1515/htmp-2016-0215.

[15] A. Stefanik, P. Szota, S. Mróz, T. Bajor, H.J.Ao.M. DyjaMaterials, Properties of the AZ31 Magnesium Alloy Round Bars Obtained in Different Rolling Processes / Własności Prętów Okrągłych Ze Stopu Magnezu AZ31 Otrzymanych W Różnych Procesach Walcowania, 60 (2015) 3001-3006. https://doi.org/10.1515/amm-2015-0479. .

[16] M. Diez, H.E. Kim, V.N. Serebryany, S.V. Dobatkin, Y.J.M.S. EstrinMicrostructure, Processing, Improving the mechanical properties of pure magnesium by three-roll planetary milling, 612, 2014, pp. 287–292. https://doi.org/10.1016/j.msea.2014.06.061..

[17] A. Stefanik, A. Morel, S. Mróz, P.J.Ao.M. SzotaMaterials, Theoretical And Experimental Analysis Of Aluminium Bars Rolling Process In Three-High Skew Rolling Mill, 60, 2015, pp. 809-813. https://doi.org/10.1515/amm-2015-0211..

[18] T.K. Akopyan, Y.V. Gamin, S.P. Galkin, A.S. Prosviryakov, A.S. Aleshchenko, M. A. Noshin, A.N. Koshmin, A.V. Fomin, Radial-shear rolling of high-strength aluminum alloys: finite element simulation and analysis of microstructure and mechanical properties, Mater. Sci. Eng.: A 786 (2020) 139424, https://doi.org/10.1016/j.msea.2020.139424.

[19] A. Arbuz, A. Kawalek, K. Ozhmegov, H. Dyja, E. Panin, A. Lepsibayev, S. Sultanbekov, R. Shamenova, Using of radial-shear rolling to improve the

structure and radiation resistance of zirconium-based alloys, Materials (Basel) 13 (19) (2020), https://doi.org/10.3390/ma13194306.

[20] M.M. Skripalenko, S.O. Rogachev, V.E. Bazhenov, B.A. Romantsev, M. N. Skripalenko, B.V. Karpov, A.Y. Titov, A.V. Koltygin, A.V. Danilin, Research of three-high screw rolling of aluminum billets with copper inserts at different rolls feed angles, Metals (2023), https://doi.org/10.3390/met13101671.

[21] A. Arbuz, A. Kawalek, K. Ozhmegov, H. Dyja, E. Panin, A. Lepsibayev, S. Sultanbekov, R. Shamenova, Using of radial-shear rolling to improve the structure and radiation resistance of zirconium-based alloys, Materials (2020), https://doi.org/10.3390/ma13194306.

[22] A. Naizabekov, S.N. Lezhnev, A.S. Arbuz, E. PaninThe effect of radial-shear rolling on microstructure and mechanical properties of stainless austenitic steel AISI-321, 2018. https://doi.org/https://doi.org/10.1051/matecconf/201819011003..

[23] A. Naizabekov, S. Lezhnev, A. Arbuz, E.J.M.W.C. PaninThe effect of radial-shear rolling on microstructure and mechanical properties of stainless austenitic steel AISI-321, 190, 2018, 11003. https://doi.org/10.1051/matecconf/201819011003..

[24] T.K. Akopyan, N.A. Belov, A.S. Aleshchenko, S.P. Galkin, Y.V. Gamin, M. V. Gorshenkov, V.V. Cheverikin, P.K. Shurkin, Formation of the gradient microstructure of a new Al alloy based on the Al-Zn-Mg-Fe-Ni system processed by radial-shear rolling, Mater. Sci. Eng.: A 746 (2019) 134–144, https://doi.org/10.1016/j.msea.2019.01.029.

[25] Y.V. Gamin, A. Koshmin, T.Y. Kin, A.J.M.T.P. AleshchenkoComparative analysis of stress-strain state of bars from aluminum alloys A2024 and A7075 processed by RSR based on FEM modeling, 46 (2021) 8138–8142, 10.1016/j. matpr.2021.03.106..

[26] X.Y. Zhang, R. Wang, X.G. Wang, Research on hot deformation behaviors of 6061 Al alloy, Mater. Sci. Forum Trans. Tech. Publ. (2021) 141–146, https://doi.org/10.4028/www.scientific.net/MSF.1032.141.

[27] V. Yashin, S. Ruschits, E. Aryshensky, I.J.T.M. LatushkinRheol. Behav. 01570 AA5182 Wrought Alum. Alloy. hot Deform. Cond. 3 (2019) 53–58, 10.17580/tsm.2019.03.09..

[28] Y. Gamin, T. Akopyan, A. Koshmin, A. Dolbachev, A. Aleshchenko, S.P. Galkin, B. A.J.T.I.Jo.A.M.T. RomantsevInvestigation of the microstructure evolution and properties of A1050 aluminum alloy during radial-shear rolling using FEM analysis, 108 (3) (2020) 695–704, 10.1007/s00170-020-05227-8..

[29] S.P. Galkin, Y.V. Gamin, T.Y.J.M. Kin, 2022, Analysis of Temperature Influence on Strain-Speed Parameters of Radial-Shear Rolling of Al-Zn-Mg-Ni-Fe Alloy, 15(20), 2022, 7202. https://doi.org/10.3390/ma15207202.

[30] J.C. Williams, E.A.J.Am Starke JrProgress in structural materials for aerospace systems, 51(19), 2003, pp. 5775–5799, 10.1016/j.actamat.2003.08.023..

[31] A.B. Naizabekov, S.N. Lezhnev, E.J.S.S.P. PaninFormation of a gradient structure in austenitic stainless steel AISI 321 by radial-shear rolling, 316, 2021, pp. 246-251. https://doi.org/10.4028/www.scientific.net/SSP.316.246..

[32] A. Stefanik, P. Szota, S. Mróz, T. Bajor, H.J.Ao.M. Dyja, 2015, Materials, Properties of the AZ31 magnesium alloy round bars obtained in different rolling processes, 60 (4), 2015.

[33] P. Shurkin, T. Akopyan, S. Galkin, A.J.M.S. AleshchenkoH. Treatment, Effect of radial shear rolling on the structure and mechanical properties of a new-generation high-strength aluminum alloy based on the Al–Zn–Mg–Ni–Fe system, 60, 2019, pp. 764-769. https://doi.org/10.1007/s11041-019-00353-x..

[34] T. Akopyan, Y. Gamin, S. Galkin, A. Koshmin, T. Kin, V. Cheverikin, A.J.Jo.M.S. AleshchenkoEffect of process parameters on the microstructure and mechanical properties of bars from Al-Cu-Mg alloy processed by multipass radial-shear rolling, 57(17), 2022, pp. 8298-8313. https://doi.org/10.1007/s10853-022-07167-y..

[35] Y.V. Gamin, A. Koshmin, A. Dolbachev, S. Galkin, A. Aleschenko, M.J.R.Jo.N.-F.M. KadachStudying the influence of radial-shear rolling on thermal deformation

conditions of A1050 processing, 61, 2020, pp. 646–657, 10.3103/S1067821220060085..

[36] Z. Zhang, D. Liu, T. Man, N. Li, Y. Yang, Y. Pang, J.J.Ao.C. Wang, M. Engineering, Numerical and experimental investigations on Mannesmann effect of nickel-based superalloy, 22(3), 2022, 133. https://doi.org/10.1007/s43452-022-00452-2..

[37] Q. Nguyen, A.S. Aleshchenko, FEM-based comparison of mandrel wear resulting from elongation of pipes manufactured from various materials on a two-roll screw rolling mill, materials science forum, Trans. Tech. Publ. (2022) 96–101, https://doi.org/10.4028/www.scientific.net/MSF.1049.96.

[38] A. Stefanik, P. Szota, S. Mróz, M.J.M. WachowskiChanges in the properties in bimodal Mg alloy bars obtained for various deformation patterns in the RSR rolling process, 15(3), 2022, 954. https://doi.org/10.3390/ma15030954.

[39] R.L. Shatalov, E.E. Zagoskin, V.A. Medvedev, I.S. Eldeeb, Computer-aided and experimental study of temperature effect on the quality indicators of piercing mandrels when rolling steel 50 vessels on a screw-rolling mill 30–80. part 1, Metallurgist (2024), https://doi.org/10.1007/s11015-024-01725-2.

[40] S. Lezhnev, A. Naizabekov, E. Panin, A. Tolkushkin, D. Kuis, A. Kasperovich, R.J.M. YordanovaSi Engineering, Development and Computer Simulation of the New Combined Process for Producing a Rebar Profile, 2021, 2023.

[41] C.-K. Shih, C.J.Jompt Hung, Experimental and numerical analyses on three-roll planetary rolling process, 142(3), 2003, pp. 702-709. https://doi.org/10.1016/S0924-0136(03)00810-0..

[42] C.-K. Shih, C. Hung, Experimental and numerical analyses on three-roll planetary rolling process, J. Mater. Process. Technol. 142 (3) (2003) 702–709, https://doi.org/10.1016/S0924-0136(03)00810-0.

[43] Y.-M. Hwang, W.M. Tsai, F.H. Tsai, I. Her, Analytical and experimental study on the spiral marks of the rolled product during three-roll planetary rolling processes, Int. J. Mach. Tools Manuf. 46 (12) (2006) 1555–1562, https://doi.org/10.1016/j.ijmachtools.2005.09.013.

[44] Y. Gamin, T. Akopyan, A. Koshmin, A. Dolbachev, A. Aleshchenko, S.P. Galkin, B. A. Romantsev, Investigation of the microstructure evolution and properties of A1050 aluminum alloy during radial-shear rolling using FEM analysis, Int. J. Adv. Manuf. Technol. 108 (3) (2020) 695–704, https://doi.org/10.1007/s00170-020-05227-8.

[45] Y.L. Wang, A. Molotnikov, M. Diez, R. Lapovok, H.-E. Kim, J.T. Wang, Y.J.M.S. Estrin, E, A, Gradient structure produced by three roll planetary milling: numerical simulation and microstructural observations, 639 (2015) 165–172, 10.1016/j. msea.2015.04.078..

[46] A. Naizabekov, S. Lezhnev, A. Arbuz, E. Panin, Obtaining of long-length rods with ultrafine-grained structure by the radial-shear rolling, IOP Conference Series: Materials Science and Engineering, IOP Publishing, 2018, p. 012065. https://doi.org/https://doi.org/10.1088/1757-899X/461/1/012065.

[47] C. Yang, Z. Zheng, Z.J.T.I.Jo.A.M.T. Hu, 2018, Simulation and experimental study on the concavity of workpiece formed by cross wedge rolling without stub bar, 95, pp. 707-717. https://doi.org/10.1007/s00170-017-1252-7.

[48] R.Z. Valiev, R.K. Islamgaliev, I.V.J.Pims Alexandrov, Bulk. Nanostruct. Mater. Sev. Plast. Deform. 45 (2) (2000) 103–189, https://doi.org/10.1016/S0079-6425(99)00007-9.

[49] R.Z. Valiev, Y. Estrin, Z. Horita, T.G. Langdon, M.J. Zechetbauer, Y.T.J.J. Zhu, Producing bulk ultrafine-grained materials by severe plastic deformation, Nanostruct. Mater. 58 (2006) 33–39, https://doi.org/10.1007/s11837-006-0213-7.

[50] A. Arbuz, A. Kawalek, K. Ozhmegov, H. Dyja, E. Panin, A. Lepsibayev, S. Sultanbekov, R.J.M. Shamenova, Using of radial-shear rolling to improve the structure and radiation resistance of zirconium-based alloys, Materials 13 (19) (2020) 4306, https://doi.org/10.3390/ma13194306.

Efficient Formability in Radial-Shear Rolling of A2024 Aluminum Alloy with Screw Rollers

Ibrahim Saad ELDeeb*,a, Ahmed A. Hawama , Ahmed Nabhanb, Mohamed Egiza**,c,d

aDepartment of Production Engineering and Mechanical Design, Faculty of Engineering, Tanta University, Tanta, 31527, Egypt.

bProduction Engineering and Mechanical Design, Faculty of Engineering, Minia University, Minya 61111, Egypt.

cDepartment of Mechanical Engineering, Kafrelsheikh University, Kafrelsheikh 33516, Egypt.

dSchool of Engineering, Robert Gordon University, Aberdeen AB10 7GJ, UK.

Corresponding authors: *E-mail*: ibrahim.eldeeb@f-eng.tanta.edu.eg & m.egiza@rgu.ac.uk

Thermal properties of A2024 aluminium alloy, sourced from the QFORM database, served as initial conditions for the finite element (FE) simulations.
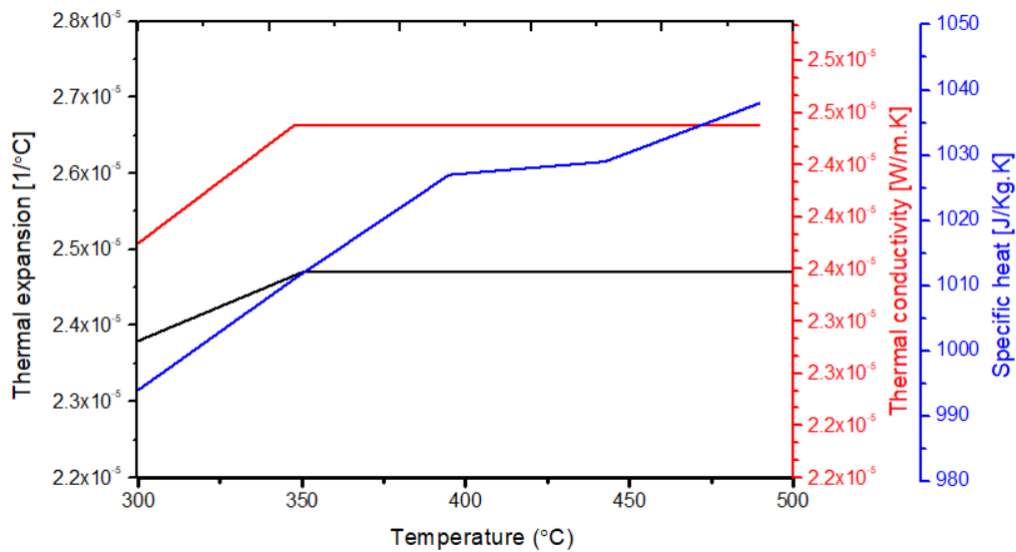

Fig. 1 Thermal properties of A2024 aluminium alloy